

Prefrontal Phase Locking to Hippocampal Theta Oscillations

Athanassios G. Siapas,^{1,3,*} Evgueniy V. Lubenov,^{2,3} and Matthew A. Wilson²

¹Computation and Neural Systems Program
Division of Biology

Division of Engineering and Applied Science
California Institute of Technology
Pasadena, California 91125

²Picower Center for Learning and Memory
Department of Brain and Cognitive Sciences
Department of Biology
Massachusetts Institute of Technology
Cambridge, Massachusetts 02139

Summary

The interactions between cortical and hippocampal circuits are critical for memory formation, yet their basic organization at the neuronal network level is not well understood. Here, we demonstrate that a significant portion of neurons in the medial prefrontal cortex of freely behaving rats are phase locked to the hippocampal theta rhythm. In addition, we show that prefrontal neurons phase lock best to theta oscillations delayed by approximately 50 ms and confirm this hippocampo-prefrontal directionality and timing at the level of correlations between single cells. Finally, we find that phase locking of prefrontal cells is predicted by the presence of significant correlations with hippocampal cells at positive delays up to 150 ms. The theta-entrained activity across cortico-hippocampal circuits described here may be important for gating information flow and guiding the plastic changes that are believed to underlie the storage of information across these networks.

Introduction

Many lines of evidence have demonstrated the critical importance of the hippocampus in the formation of new memories (Squire, 1992). This hippocampal involvement is temporary, as memories are gradually established in extrahippocampal networks through the process of memory consolidation. The predominant conjecture is that during this process hippocampal activity drives the progressive integration of new information in distributed neocortical circuits.

While the precise locus and organization of cortical memories and the neuronal mechanisms underlying their establishment remain unknown, previous studies have proposed that the prefrontal cortex plays a key role in this process (Wiltgen et al., 2004; Fuster, 1997; Fletcher and Henson, 2001). The existence of strong functional hippocampo-prefrontal interactions in the rat is supported by anatomical and electrophysiological studies that have demonstrated the existence of a

monosynaptic pathway from the hippocampus to the medial prefrontal cortex (mPFC) (Swanson, 1981; Ferino et al., 1987; Thierry et al., 2000), which is endowed with the ability to undergo activity-dependent modifications (Laroche et al., 1990; Laroche et al., 2000; Jay et al., 1995; Takita et al., 1999). Disruption of the hippocampo-prefrontal pathway has been shown to impair performance on spatial learning tasks (Floresco et al., 1997), with recent experiments also showing reverse temporal gradients in the involvement of hippocampal and prefrontal circuits (Wiltgen et al., 2004). In particular, hippocampal circuits appear to be strongly engaged in the early stages of learning and show only limited activation as learning progresses, while the reverse gradient has been documented for prefrontal circuits (Bontempi et al., 1999; Frankland et al., 2004; Maviel et al., 2004). This is further corroborated by recent experiments showing that lesions to the hippocampus of rats during trace eyeblink conditioning produce a profound deficit early in training but have little effect in the late stages of training. In contrast, mPFC lesions produce a strong deficit in the late but not in the early stages of training (Takehara et al., 2003).

These observations suggest that during the course of learning information is gradually consolidated in prefrontal circuits in a hippocampus-dependent manner. However, the basic organization of hippocampo-prefrontal interactions at the level of networks of neurons remains unknown. To make progress in characterizing these interactions, we monitored the simultaneous activity of multiple single neurons in the hippocampus and mPFC of freely behaving rats using chronic multi-tetrode recordings. Here, we focus on characterizing the timing relationships between neuronal activity in the medial prefrontal cortex and the hippocampal theta rhythm. The theta rhythm is a local field potential (LFP) oscillation in the 4–10 Hz frequency range that has long been recognized as the defining electrophysiological signature of hippocampal activity during active exploratory behavior and REM sleep (Green and Arduini, 1954; Vanderwolf, 1969; Buzsaki, 2002). Theta oscillations are known to modulate neuronal activity not only within the hippocampus (Buzsaki and Eidelberg, 1983; Fox et al., 1986), but also in subcortical (Vinogradova and Brazhnik, 1977; Kocsis and Vertes, 1992; Pedemonte et al., 1996; Natsume et al., 1999; Bassant and Poindeussous-Jazat, 2001; Gambini et al., 2002), limbic (Alonso and Garcia-Austt, 1987; Pare and Gaudreau, 1996), and cortical (Colom et al., 1988; Pedemonte et al., 2001) structures. Hence, theta oscillations appear to be a ubiquitous property of brain networks, and phase locking to theta oscillations appears to be an important organizing principle of brain activity during awake behavior and REM sleep.

Here we report, to our knowledge for the first time, that neurons in the medial prefrontal cortex are phase locked to the hippocampal theta rhythm. We quantitatively characterize and compare the basic phase locking properties of prefrontal and hippocampal cells, and we demonstrate that the observed phase locking is not

*Correspondence: thanos@caltech.edu

³These authors contributed equally to this work.

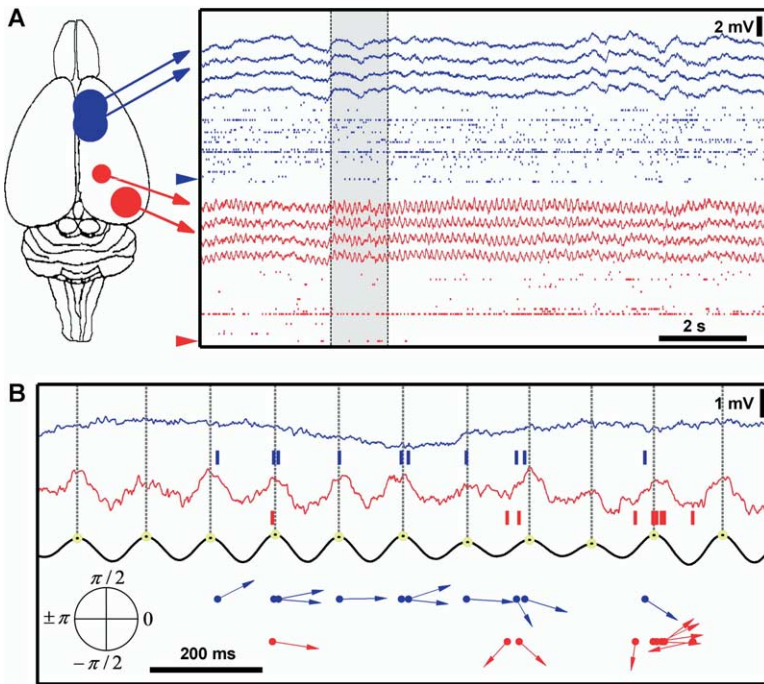


Figure 1. Examples of Theta Phase Locking (A) Four simultaneously recorded prefrontal local field potential (LFP) traces (in blue) and four hippocampal LFP traces (in red), together with rasters of single-unit activity in the prefrontal cortex (35 neurons) and hippocampus (37 neurons). The total duration of the LFP traces shown here is 13 s. The brain diagram on the left indicates the recording sites of the hippocampal (red) and prefrontal (blue) recordings. For all figures, hippocampal and prefrontal examples are shown in red and blue, respectively.

(B) The gray region in (A) expanded. A cortical LFP trace and the spike train of a prefrontal cortical neuron are shown in blue. Underneath in red is a hippocampal LFP trace and the activity of a place cell as the animal traverses its place field. The two selected neurons are marked by arrows in (A). Shown in black is the hippocampal trace band-pass filtered in the theta range (4–10 Hz). The yellow dots and the gray dotted lines indicate the position of the peaks of the theta rhythm, which were automatically identified as described in the [Experimental Procedures](#). The phase locking of the hippocampal pyramidal cell is evident. Moreover, notice that despite the lack of any apparent theta rhythmicity in the prefrontal LFP trace there is still a striking

phase locking of the prefrontal neuron to the hippocampal theta oscillation, which is recorded at a significant distance away from the prefrontal neuron (~ 7 mm). The unit vector sequences corresponding to the cortical (blue) and hippocampal (red) spike trains are shown at the bottom. Each unit vector is oriented by the phase value of its corresponding spike (peaks correspond to 0 radians, and troughs correspond to $\pm\pi$).

simply due to intrinsic rhythmicity of neuronal firing in the θ frequency band but explicitly depends on the entrainment of spiking activity to the ongoing frequency fluctuations of the hippocampal theta rhythm.

Furthermore, we show that, while hippocampal neurons phase lock best to simultaneously occurring theta oscillations, prefrontal cells phase lock best to theta oscillations delayed by approximately 50 ms. This result is consistent with a directionality in the hippocampo-prefrontal interactions, with hippocampal activity leading the activity in prefrontal cortex. This directionality is confirmed at the level of single-cell interactions. We further demonstrate that the phase locking of a prefrontal cell is strongly predicted by the presence of significant correlations with a subset of hippocampal cells over a range of positive delays up to 150 ms. This suggests that direct hippocampal input is likely to have a considerable contribution to the observed prefrontal theta phase locking. Finally, we discuss the implications of the temporal organization of cortico-hippocampal interactions demonstrated here for the channeling of information flow and the recruitment of plasticity mechanisms that are believed to underlie the storage of information.

Results

Detection of Phase Locking to Hippocampal Theta Oscillations

We recorded simultaneously local field potential (LFP) traces and single-unit activity in the hippocampus and the medial prefrontal cortex of rats performing a variety of spatial navigation tasks ([Figure 1](#)). To characterize

the timing relationship of neuronal firing to the hippocampal theta rhythm, the hippocampal LFP was first band-pass filtered in the θ band (4–10 Hz), and the filtered trace was decomposed into instantaneous amplitude $\rho(t)$ and phase $\phi(t)$ components. A spike occurring at time τ was assigned phase value $\phi(\tau)$. In this fashion, the spike train of each cell was converted into a sequence of unit length vectors oriented by the phase values of their corresponding spikes ([Figure 1](#)). The mean resultant vector was computed as the average of the vector sequence, and the mean direction or mean preferred phase was computed as the orientation of the mean resultant vector ([Experimental Procedures](#)).

Intuitively, if the firing of a given neuron is independent of the theta rhythm, the distribution of its phase values will be random, i.e., uniform on $[-\pi, +\pi]$, and its mean resultant vector will be short. Conversely, if the firing of a given neuron is phase locked to the theta rhythm, its phase value distributions will be unimodal, and its resultant vector will be long. The significance of phase locking can thus be evaluated using Rayleigh's Z statistic, which is directly related to the length of the mean resultant vector ([Experimental Procedures](#)).

Population Analysis of Prefrontal and Hippocampal Theta Phase Locking

Approximately 80% of hippocampal cells and 40% of prefrontal cells that we recorded were significantly phase locked to the hippocampal theta rhythm ([Figure 2](#)). The proportions of phase-locked cells varied very little with respect to the phase extraction method (typical standard error of the mean less than 1%). Since

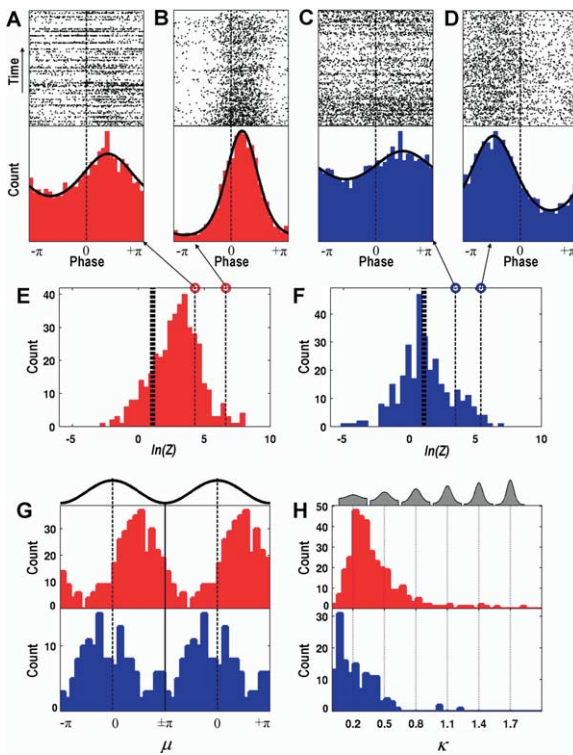


Figure 2. Theta Phase Locking of Hippocampal and Prefrontal Neurons

(A–D) Examples of phase locking to the hippocampal theta rhythm for two hippocampal units (A and B) and two prefrontal cortical units (C and D). The spike trains of individual units were broken up at the troughs of the hippocampal theta rhythm and the resulting segments were stacked up to form the theta-triggered rasters shown on top. Below are the corresponding phase value distributions. Also shown are the von Mises fits for each example parameterized by mean direction μ and concentration parameter κ . Parameter pairs (μ , κ) are as follows: (A) (1.18, 0.33); (B) (0.60, 1.42); (C) (1.50, 0.19); (D) (–1.47, 0.61).

(E and F) Distribution of log-transformed Rayleigh's Z, the statistic used to evaluate the significance of phase locking for hippocampal (E) and prefrontal (F) units. Significance probability associated with Z (based on 50 spikes or more) is $p \approx e^{-Z}$, and therefore $\ln(Z) \approx \ln(-\ln(p))$. Thick black lines indicate the $p = 0.05$ significance threshold, thus all values of $\ln(Z)$ to the right of these lines are significant at that confidence level. Note that the logarithmic transformation is applied to tighten the Z distribution, yielding a double logarithmic scale, so that $\ln(Z)$ values [1, 2, 3, 4, 5] approximately correspond to p values [10^{-1} , 10^{-3} , 10^{-9} , 10^{-24} , 10^{-64}]. 80.85% \pm 0.63% (332 \pm 2.6 out of 411) of hippocampal and 44.03% \pm 0.50% (139 \pm 1.6 out of 316) of prefrontal units were phase locked to the hippocampal theta rhythm ($p = 0.05$). When analysis is restricted to unique single units, the corresponding figures are 81.34% \pm 1.84% (90 \pm 2 out of 111) and 34.77% \pm 0.63% (39 \pm 0.7 out of 113) for the hippocampus and prefrontal cortex, respectively. The displayed distributions are based on phase extraction using the analytic signal method, while the means and their associated standard errors result from averaging over values based on seven complementary phase extraction methods (see [Experimental Procedures](#)).

(G) Histograms of mean preferred phase μ for all significantly phase-locked hippocampal (top) and prefrontal (bottom) units independent over two theta cycles for visual clarity. Most hippocampal units have preferred phase on the falling edge of the theta cycle ($\bar{\mu} = 1.54$, circular variance 0.54), while the prefrontal population displays a wider distribution centered around the peak ($\bar{\mu} = -0.60$, circular variance 0.72). The distributions offer only qualitative description, since units from different animals were referenced against LFP signals not necessarily derived from precisely the same depth in the

the presence of phase locking only indicates departure from uniformity in the phase value distribution of a given cell, we further characterized the locking properties of individual units by fitting von Mises densities to their corresponding phase value distributions (Figures 2A–2D).

The von Mises distribution is the circular analog of the normal distribution and is parameterized by a mean direction or preferred phase, μ , and concentration parameter, κ , with larger κ values corresponding to more peaked distributions ([Experimental Procedures](#)). As has been previously reported, most hippocampal neurons had preferred phases on the falling edge of the theta cycle (Figure 2G) resulting in a unimodal μ distribution (Fox et al., 1986; Buzsaki, 2002). In contrast, the prefrontal distribution of preferred phases relative to the hippocampal theta oscillations was wider and centered close to the peak of the theta cycle. It should be noted that the theta rhythm was always extracted from a particular tetrode in each animal, and it was therefore nonlocal to the majority of the recorded cells. Neurons in both areas displayed a broad range of degrees of phase locking and corresponding κ values, with the hippocampal population exhibiting a tendency toward more concentrated phase value distributions compared to the prefrontal one (Figure 2H).

Phase Locking Dependence on the Microstructure of the Theta Rhythm

Since the theta rhythm is an oscillatory process constrained to a narrow frequency band (4–10 Hz), it is important to show that the phase locking properties described above do not arise simply from intrinsic rhythmicity in the firing of hippocampal and prefrontal neurons in the same frequency range. Theta oscillations are not constant in frequency but show a pattern of small frequency fluctuations over time, which we refer to as the *microstructure* of the theta rhythm. Because of such frequency fluctuations, a neuron with rhythmic firing at a fixed frequency in the θ range will not necessarily show phase locking, and conversely, a significantly phase-locked neuron will not necessarily reveal itself to be rhythmic as defined by autocorrelation or interspike interval measures. For significant phase locking to be present, the spike train of a given

hippocampus, therefore introducing a potential phase offset that likely shifts and broadens the overall distribution of preferred phases.

(H) Histograms of phase value distribution concentration parameters κ for significantly phase-locked hippocampal (top) and prefrontal (bottom) units. The gray von Mises distributions shown on top visually indicate the degree of modulation corresponding to six labeled concentration parameter values. The hippocampal population is biased toward more concentrated phase value distributions ($\bar{\kappa} = 0.39$, $\sigma_{\kappa} = 0.26$) than the prefrontal population ($\bar{\kappa} = 0.24$, $\sigma_{\kappa} = 0.20$). The phase value distributions of 85% of the prefrontal units and 61% of the hippocampal units were fit well by the von Mises density (U^2 goodness of fit test, $p = 0.05$). In most remaining cases, the fit was imperfect due to subtle deviations in the phase value distribution such as the presence of slight asymmetry, rather than due to drastic model departures such as multimodality. Altogether, κ captured well the degree of modulation in the phase value distributions.

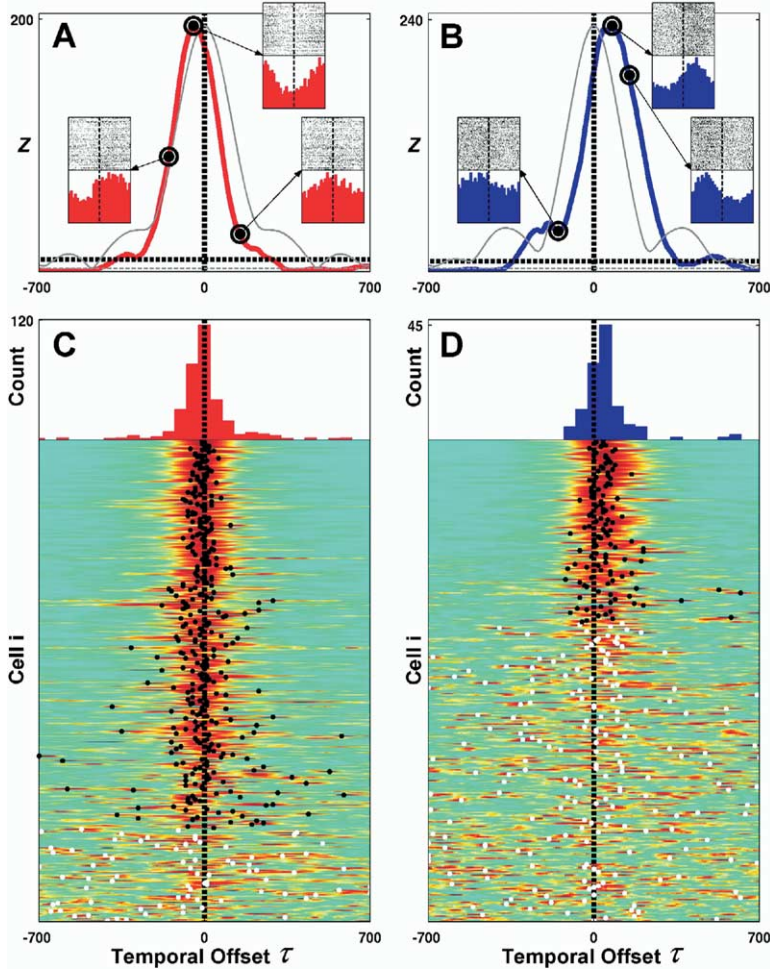


Figure 3. Timing Relationships between Phase-Locked Neurons and the Theta Rhythm

(A and B) Rayleigh's Z computed as a function of temporal offset τ between the hippocampal theta trace and the spike train of a hippocampal (A) and a prefrontal cortical (B) neuron ($\tau > 0$ indicates shifting the spike train back in time or equivalently shifting the theta trace forward). Behind in gray are the scaled envelopes of the autocorrelation functions of the filtered hippocampal theta traces used in each example. Note the rapid decay in Z value and autocorrelation with increase in temporal offset. The inserts show explicitly the theta-triggered rasters and phase value distributions at temporal offsets $\tau = -150, -45.89, 150$ ms for (A) and $\tau = -150, 78.40, 150$ ms for (B). Z decays at a similar rate as the reference theta traces decorrelate, and sufficiently large time offsets ($|\tau| > 1$ s) abolish the significance of the phase locking. This demonstrates that the observed phase locking explicitly depends on the entrainment of neuronal firing to the ongoing frequency fluctuations of the hippocampal theta rhythm. Note that in these examples the hippocampal unit was maximally phase locked to the future of the LFP signal (i.e., at $\tau = -45.89 < 0$), while the prefrontal unit was maximally phase locked to the past of the LFP signal (i.e., at $\tau = 78.40 > 0$).

(C and D) Pseudocolor panels show analysis as in (A) and (B) carried out for all hippocampal (C) and prefrontal (D) units. Rayleigh's Z as a function of temporal offset τ for each unit is normalized by its maximal value Z_{max} occurring at τ_{max} , color coded, and displayed in a row. Rows are sorted by Z_{max} in descending order. Black and white dots indicate the location of τ_{max} , and the color signi-

ifies whether (black) or not (white) Z_{max} exceeded the significance threshold. The significance threshold was elevated to $p = 0.05/141$, since a hypothesis test can be thought to occur at each of the 141 temporal offset values (τ varied between -700 and $+700$ ms in 10 ms increments). 330 out of 411 hippocampal and 120 out of 316 prefrontal units had above threshold Z_{max} . Note that the significance of phase locking of these units tends to decay at a similar rate, as can be witnessed by the uniform thickness of the red band along the red band along the midline. Also, note that the red band and τ_{max} occur along the zero offset midline for the hippocampal population (C) but are clearly shifted to a positive offset for the prefrontal population (D). This is explicitly demonstrated in the histograms above showing the distributions of the significant τ_{max} (black dots) for the hippocampal population ($\bar{\tau}_{max} = -3.94 \pm 7.15$ ms) and the prefrontal population ($\bar{\tau}_{max} = 49.92 \pm 10.76$ ms). Hippocampal units were therefore maximally phase locked to the present of the hippocampal theta rhythm, while the prefrontal units were maximally phase locked to its past.

neuron must match the microstructure of the theta rhythm. This implies that perturbing the temporal alignment between the theta rhythm and a spike train should decrease the degree of phase locking in proportion to the size of the perturbation. We confirmed this explicitly by showing that the degree of phase locking computed at different temporal offsets between the theta rhythm and neuronal spike trains decays with increasing offsets (Figure 3). Temporal offsets of 1 s or more abolish the statistical significance of phase locking, rendering the phase value distributions close to uniform for both hippocampal (Figures 3A and 3C) and prefrontal (Figures 3B and 3D) neurons. Note that introducing a temporal offset between the theta rhythm and a given spike train affects only the joint statistics of these two processes without affecting the statistics of the processes themselves. This analysis establishes that the observed phase locking is not simply due to intrinsic rhythmicity

of neuronal firing in the θ frequency band but explicitly depends on the entrainment of spiking activity to the ongoing frequency fluctuations of the hippocampal theta rhythm.

Maximal Neuronal Phase Locking Occurs for Time-Shifted Hippocampal Theta Oscillations

A striking aspect of Figure 3 is that maximal phase locking need not occur when the spike train and the LFP trace are aligned, i.e., at time offset $\tau = 0$. For example, the hippocampal cell (Figure 3A) is maximally locked to the hippocampal theta rhythm shifted back in time ($\tau_{max} = -45.89$ ms), while the prefrontal cell is maximally locked to the theta rhythm shifted forward in time ($\tau_{max} = 78.40$ ms). In other words, the example hippocampal cell is maximally locked to the future of the LFP signal, while the prefrontal cell is maximally locked to its past. This observation is consistent with

the interpretation that the current sources and sinks associated with the firing of this hippocampal cell contribute to the LFP signal, while the firing of this prefrontal cell is influenced by theta-modulated hippocampal outputs after some delay.

At the population level, the hippocampal distribution of offsets τ_{\max} yielding maximal phase locking was centered around zero offset ($\bar{\tau}_{\max} = -3.94 \pm 7.15$ ms) and exhibited marked variability ($\sigma_{\tau_{\max}} = 129.96$ ms) (Figure 3C). In contrast, the prefrontal distribution of τ_{\max} was centered at a positive offset ($\bar{\tau}_{\max} = 49.92 \pm 10.76$ ms) and exhibited similar variability as the hippocampal population ($\sigma_{\tau_{\max}} = 117.41$ ms) (Figure 3D). The prefrontal population mean $\bar{\tau}_{\max}$ was significantly different from 0, with mean z score of 4.25 averaged over the different phase extraction methods.

One might hypothesize that the time offset associated with maximal locking depends on the preferred phase and/or concentration parameter of a given cell. We examined this hypothesis explicitly by fitting a circular regression for τ_{\max} and μ and a standard linear regression for τ_{\max} and κ but did not detect any significant interaction ($p = 0.05$). Thus, the time offset associated with maximal locking appears to be an independent dimension along which neuronal activity can be characterized and studied.

Covariance between Prefrontal and Hippocampal Cells Indicates Directionality in Hippocampo-Prefrontal Interactions

The fact that prefrontal cells phase lock best to time-delayed theta oscillations (Figure 3D) suggests that prefrontal firing is influenced by theta-modulated hippocampal inputs after a mean delay of approximately 50 ms. To examine this hypothesis more directly at the single-cell level, we computed the cross-covariance functions between all pairs of simultaneously recorded prefrontal and hippocampal cells. This analysis revealed that a specific subset of prefrontal cells indeed had significant correlations with subsets of the simultaneously recorded hippocampal cells at positive lags up to 150 ms, consistent with the directionality and mean lag predicted by the analysis of the previous section (Figure 4).

The interactions of each prefrontal cell i with the population of simultaneously recorded hippocampal cells were summarized through the standardized mean cross-covariance $Q_i(u)$ (Figures 4D and 4H; Experimental Procedures). Approximately 10% of the prefrontal units displayed mean cross-covariance structure similar to the one exemplified in Figures 4D and 4H, i.e., having one very significant 50–100 ms wide peak or trough, occupying a range of positive lags up to 150 ms. The rest of the units did not exhibit any clear cross-covariance structure but instead had much narrower, less prominent peaks and troughs, distributed over the entire range of positive and negative lags. We confirmed that most of the latter were spurious cross-covariances, an expected artifact arising in connection with low mean firing rates, that disappeared almost completely when the analysis was restricted to cell pairs with sufficient number of spikes (see Experimental Procedures).

Covariance between Prefrontal and Hippocampal Cells Predicts Prefrontal Phase Locking

To explore the possible contribution of hippocampal inputs to prefrontal theta phase locking, we compared the mean cross-covariances of phase-locked prefrontal units (Figure 4J) and non-phase-locked prefrontal units (Figure 4L). Essentially all prefrontal units that had a significant cross-covariance peak or trough at positive lags up to 150 ms were phase locked (Figure 4J), while none of the units that were not phase locked exhibited an equivalent cross-covariance feature (Figure 4L). This was confirmed further by comparing the average cross-covariance across all phase-locked units, $\langle Q_i(u) \rangle_L$, with the corresponding average taken over all non-phase-locked cells, $\langle Q_i(u) \rangle_{\bar{L}}$ (Figure 4M). The average cross-covariance of the phase-locked cells had a prominent peak between 40 and 120 ms and a smaller trough between -125 and -100 ms. Furthermore, it was significantly different from the average cross-covariance of the non-phase-locked cells in those intervals (Figure 4M). This was consistent with the interpretation that the firing of hippocampal units influenced the firing of phase-locked prefrontal units.

We also confirmed that the apparent absence of prominent features in the cross-covariances of non-phase-locked units (Figure 4L) was not due to the potential negation of significant features of opposite sign that could have occurred in the computation of individual $Q_i(u)$ (Figures 4D and 4H). In particular, for each prefrontal cell we computed the mean squared cross-covariance, $Q_i^2(u)$, a nonnegative measure of the significance of the interactions as a function of lag and independent of sign. The average $Q_i^2(u)$ across the population of non-phase-locked units was indeed essentially flat and significantly different from the corresponding average taken across the phase-locked units, which showed a prominent peak between 20 and 120 ms (Figure 4N).

Thus, the presence of significant interactions at positive lags up to 150 ms in the mean cross-covariance of a prefrontal unit with the hippocampal population was a perfect predictor of phase locking for that prefrontal cell. Such significant cross-covariances were not observed for all phase-locked prefrontal units, which could simply be due to the limited sampling of the hippocampal population. These results suggest that direct hippocampal input contributes significantly to the observed prefrontal theta phase locking and may indeed be required.

Discussion

In summary, we presented evidence that the firing of a significant fraction of prefrontal neurons is modulated by the hippocampal theta rhythm. This prefrontal theta phase locking was present even when there was little apparent theta power in the prefrontal LFPs (Figure 1). The current sources and sinks in mPFC arising in connection with phase locking to the hippocampal theta rhythm may not contribute significantly to the θ band of the cortical LFP for several reasons. First, the relevant current generators within mPFC might have a random spatial arrangement, therefore giving rise to “closed

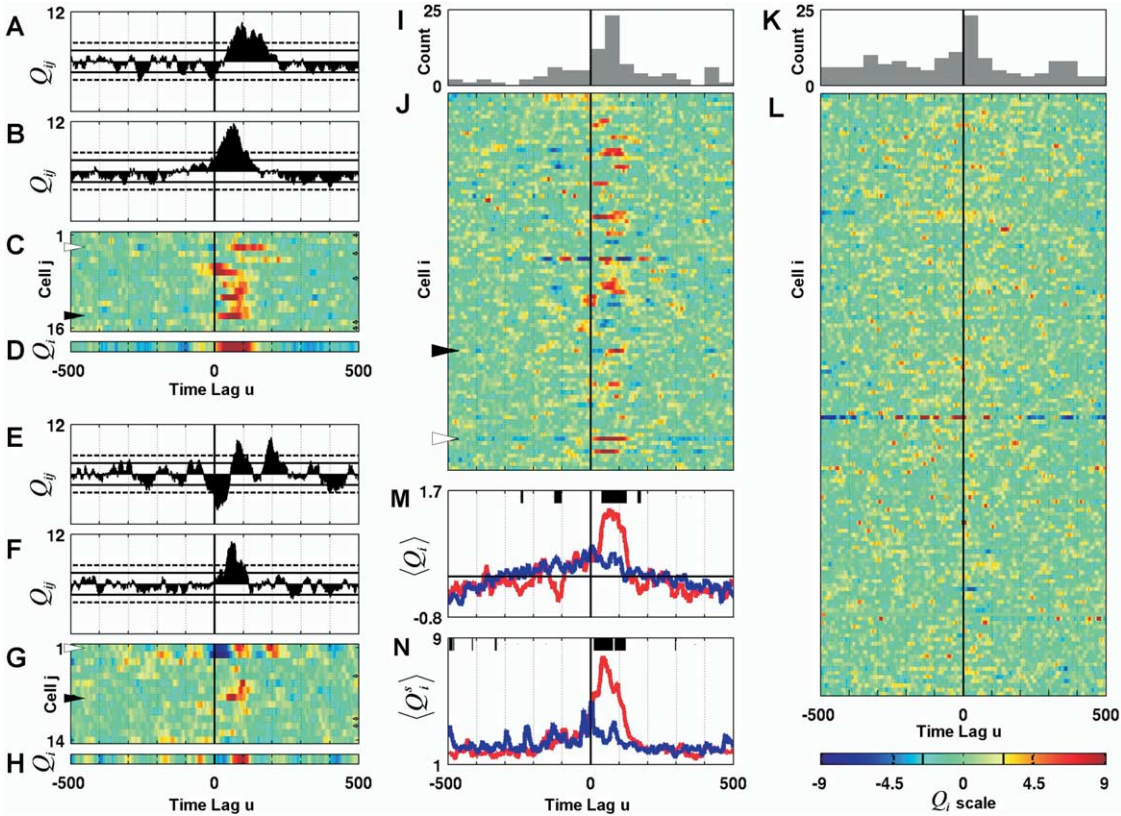


Figure 4. Cross-Covariance between Prefrontal and Hippocampal Cells Predicts Prefrontal Phase Locking

(A and B) Standardized cross-covariance $Q_{ij}(u)$ between prefrontal unit i and two simultaneously recorded hippocampal units (A) $j = 4$, (B) $j = 7$ ($u > 0$ indicates shifting unit i back in time or equivalently shifting unit j forward). The solid and dashed horizontal lines indicate the 99% and 99.999% confidence limits under the assumption of independence. If $Q_{ij}(u)$ crosses one of the dashed horizontal lines, the hypothesis of independence can be rejected at $\alpha = 0.01$. Note the prominent peaks in (A) and (B), indicating that the given prefrontal unit had a significantly elevated probability of firing between 50 and 150 ms after hippocampal unit 4 and between 0 and 100 ms after hippocampal unit 7.

(C) Each row in the pseudocolor plot shows $Q_{ij}(u)$ between the given prefrontal unit i and one of the 16 hippocampal units j that were simultaneously recorded. Examples (A) and (B) are marked by the white and black arrows on the left. Note that the peak in the cross-covariance occurs at different positive lags between 0 and 150 ms for the different hippocampal units and that there are some hippocampal units that show no significant interaction with the given mPFC unit, i.e., $j = 15$ and $j = 16$.

(D) Standardized mean cross-covariance $Q_i(u)$ between the given prefrontal unit and the population of hippocampal units (see [Experimental Procedures](#)). The pairwise cross-covariances $Q_{ij}(u)$ that are not significantly different from 0, marked with gray arrows on the right of (C), do not enter in the computation of $Q_i(u)$.

(E–H) Plots similar to (A)–(D) showing $Q_{ij}(u)$ between another prefrontal unit and all 14 hippocampal units that were simultaneously recorded. Note the more complex, multimodal structure of $Q_{ij}(u)$ and the significant dip around 0 ms in (E). While unit $j = 2$ displays cross-covariance structure similar to that of unit $j = 1$, unit $j = 8$, shown in (F), exhibits a unimodal peak around 50 ms, similar to (B). Finally, note that the dip around 0 ms is attenuated in the standardized mean cross-covariance (H), indicating that cancellation of significant cross-covariance structure of opposite sign is possible in $Q_i(u)$.

(I–L) Each row in the pseudocolor panels (J and L) shows a standardized mean cross-covariance, $Q_i(u)$, between a given prefrontal unit i and the population of hippocampal units. All significantly phase-locked prefrontal units are stacked in (J), and all remaining prefrontal units are stacked in (L). The examples from (D) and (H) are indicated by the white and black arrows on the left in (J). (I) and (K) show the distribution of time lags, u_i^{\max} , at which each of the shown $Q_i(u)$ in (J) and (L), respectively, achieved their maximal absolute values (50 ms bins). Note that many $Q_i(u)$ of the phase-locked units showed significant peaks at positive time lags up to 150 ms, as can be witnessed by the prominent red patches to the right of the midline in (J). This tendency is also reflected in the peak of the 50–100 ms bin in the distribution of u_i^{\max} shown above. The non-phase-locked population showed a tendency for peak absolute values between 0 and 50 ms, as can be seen in (K), but no salient cross-covariance features were discernible in (L).

(M) The average $Q_i(u)$ for all significantly phase-locked units $i \in L$, $\langle Q_i(u) \rangle_L$, is shown in red, and the average $Q_i(u)$ for all remaining units $i \in L$, $\langle Q_i(u) \rangle_{\bar{L}}$, is shown in blue. Thus, the red curve is the average of all rows in (J), while the blue curve is the average of all rows in (L). The black intervals at the top of the panel indicate the corresponding ranges of lags over which $\langle Q_i(u) \rangle_L$ and $\langle Q_i(u) \rangle_{\bar{L}}$ were significantly different ($p = 0.95$, Behrens-Fisher test). Note the significant peak of $\langle Q_i(u) \rangle_L$ between 40 and 120 ms and the dip between -125 and -100 ms. Both features indicate that the phase-locked mPFC units tended to discharge after the hippocampal units.

(N) $\langle Q_i^s(u) \rangle_L$ is shown in red, and $\langle Q_i^s(u) \rangle_{\bar{L}}$ is shown in blue (see [Experimental Procedures](#)). Note that $\langle Q_i^s(u) \rangle_L$ is relatively flat and significantly different from $\langle Q_i^s(u) \rangle_{\bar{L}}$ between 20 and 120 ms, demonstrating that the absence of structure in (L) is not due to the cancellation of significant features of opposite sign that might have occurred in the computation of the individual $Q_i(u)$. Thus, the prefrontal units that were not phase locked indeed did not display significant cross-covariance structure with the hippocampal units over ± 500 ms time lags.

fields” (Buzsaki, 2002). While this is possible for inputs terminating on prefrontal interneurons, it is less likely to be the case for pyramidal cells, given the characteristic parallel organization of their dendrites and afferents. Second, inputs to different phase-locked neurons might arrive over different phases of the theta cycle, eliminating the synchrony required for a prominent LFP oscillatory mode. The fact that the mean preferred phase distribution of phase-locked prefrontal cells was nonuniform argues against this hypothesis (Figure 2G). Third, the layer of prefrontal cortex yielding the highest number of single-unit data might be close to the null point of the prefrontal theta dipole. If so, the apparent absence of theta power in the prefrontal LFPs could be explained by the bias in the placement of the recording electrodes. Fourth, hippocampo-prefrontal feed-forward inhibition rather than excitation might be the major contributor to the observed phase locking. We discuss how this can explain prefrontal phase locking even in the absence of θ power in prefrontal LFPs in the section below. Finally, the presence of clear but short-lived theta oscillations in prefrontal LFPs (data not shown) argues that the mPFC circuitry can generate macroscopically observable theta oscillations but that these oscillations have more complex behavioral correlates than the hippocampal theta rhythm (Kahana et al., 1999).

As noted in the section describing the dependence of phase locking on the microstructure of the theta rhythm, phase-locked cells need not be rhythmic, and conversely, rhythmic cells need not be phase locked (Pedemonte et al., 1996). In addition, neuronal firing rate, within the physiologically relevant range, imposes no constraints on phase locking properties either. Thus, phase locking reflects an independent dimension along which neuronal activity varies and can therefore be quantified and studied. Taken together, these observations suggest that the prefrontal phase locking reported here represents an aspect of cortical neuronal activity that can be robustly quantified and studied only by direct comparison with simultaneous electrophysiological activity in the hippocampus.

Mechanisms Responsible for Prefrontal Phase Locking

Our results show the presence of directionality in hippocampo-prefrontal interactions with hippocampal activity leading activity in prefrontal cortex on average by 50 ms (Figures 3 and 4). In addition, all prefrontal cells that showed significant correlations with the hippocampal cells over a range of positive lags up to 150 ms were phase locked (Figure 4). These data suggest that the direct hippocampo-prefrontal pathway plays a crucial role in entraining prefrontal neuronal discharges to the hippocampal theta rhythm. This glutamatergic pathway has a conduction velocity of approximately 0.6 m/s and corresponding mean conduction delay of 16 ms (Ferino et al., 1987; Jay et al., 1992). In addition to the monosynaptic activation mediated via the above pathway, there is evidence for polysynaptic activation of prefrontal pyramidal neurons in response to CA1 stimulation with corresponding latency of 40 ms (De-genetals et al., 2003). The broad range of delays over

which significant hippocampo-prefrontal single-cell correlations were observed suggests that both monosynaptic and polysynaptic activation contributed to the entrainment of prefrontal cells to the hippocampal theta rhythm.

Recent evidence has demonstrated that CA1/subiculum neurons form monosynaptic excitatory connections not only with prefrontal pyramidal cells, but also with several classes of interneurons in mPFC (Tierney et al., 2004). This feed-forward inhibition has a latency slightly smaller than that of the monosynaptic hippocampo-prefrontal excitatory input. This fact suggests the intriguing possibility that phase locking in mPFC might arise, at least in part, not only through theta-modulated excitatory drive to pyramidal cells, but also through the modulation of prefrontal pyramidal cell excitability, mediated via the local inhibitory network. This could also help explain prefrontal phase locking even in the apparent absence of theta power in prefrontal LFPs. If a major portion of the theta-modulated output from the hippocampus terminates on prefrontal interneurons rather than on pyramidal cells, the rhythmic synaptic currents that it generates are unlikely to add up to a macroscopic field oscillation, because of the random geometric arrangement of interneuronal dendrites and their relatively small size. In turn, the rhythmic inhibitory output of the interneurons will tend to generate synaptic currents of relatively small amplitudes and variable polarity, dependent on the activation state of the pyramidal cells, since the reversal potential of the relevant GABA_A conductance is close to the membrane resting potential. Thus, rather than hyperpolarizing pyramidal cells, the hippocampo-prefrontal feed-forward inhibition can act to rhythmically decrease pyramidal cell input impedance, thus theta modulating their excitability.

Our evidence for direct hippocampal involvement in prefrontal phase locking is only correlative, and identifying the precise circuit mechanisms that are responsible for the theta modulation of prefrontal firing is an important open problem raised by the results presented here. There are several mechanisms that could be responsible for the observed phenomena, beyond the possibility of direct rhythmic hippocampal input to prefrontal circuits. In particular, both hippocampal and cortical cells could be comodulated at θ frequency from subcortical structures, or both comodulation and direct hippocampal rhythmic input could be contributing to the observed effect. Furthermore, resonant properties of individual cells may modulate theta phase locking properties (Leung and Yu, 1998; Chapman and Lacaille, 1999; Hu et al., 2002; Hutcheon and Yarom, 2000). These resonant properties may be controlled through external levels of neurotransmitters, and phase locking may thus be due to a combination of a permissive/modulating action and pacemaker rhythmic interactions.

Possible Functional Consequences of Prefrontal Phase Locking

The demonstrated phase locking of prefrontal neurons to the hippocampal theta rhythm represents a timing relationship that may have important consequences for

the organization of network activity over both short and long timescales.

Over short timescales, i.e., in the order of several theta cycles, phase locking can introduce consistent temporal ordering of the excitability windows of phase-locked neurons that can be utilized for directing flow and maintaining activity in neuronal networks. Given two reciprocally connected neurons whose excitability is modulated by the same oscillatory rhythm, but with a given phase offset, the sensitivity of each neuron to the outputs of the other will be differentially affected. Thus, the neuron whose excitability window precedes that of the other will be more likely to drive its target effectively. Reversing the phase offset of the modulatory rhythm will reverse the effective direction of activity flow. Elaborating on this simple model, one can see how a rhythmic modulatory influence acting on several interconnected brain regions via variable delays can gate inputs and outputs and determine the direction of activity flow. Furthermore, if several such regions are interconnected so that the sum of transmission and activation delays over a return path is in the order of 150 ms, theta phase locking can stimulate the emergence of resonant phase-locked loops. Such resonant loops have been previously hypothesized to be important for the formation and retrieval of memories across cortico-hippocampal circuits (Miller, 1991).

Over longer timescales, phase locking can introduce consistency in the relative timing of firing within subsets of coactivated prefrontal and hippocampal cells. Because of the properties of spike timing-dependent plasticity (STDP) (Markram et al., 1997; Roberts and Bell, 2002), such consistency would produce a tendency toward the selective strengthening of synapses from cells with earlier preferred phases to cells with later preferred phases, as well as toward the weakening of synapses between cells with the opposite phase relation. This would stimulate the natural formation of the resonant loops discussed above across cortico-hippocampal networks (Miller, 1991). Loop membership would be uniquely determined by the pattern of neuronal coactivation, driven by the external input and hence uniquely representing the experience of the animal. Thus, phase locking may be important for the formation of long-term memories, and quantifying the dynamics of phase locking properties associated with learning may be a way of identifying functionally important cortical neuronal assemblies, which may not be accessible by analyzing firing rate profiles alone.

Experimental Procedures

Behavioral Tasks

Recordings were obtained while rats performed a variety of spatial tasks in familiar environments. The tasks were 20–90 min long and included spatial working memory on an eight-arm maze, a delayed alternation on a T maze, and exploration of linear and circular tracks.

Electrophysiological Recordings

Electrophysiological signals were obtained using the technique of tetrode recordings (Wilson and McNaughton, 1993). Four male Long-Evans 3- to 7-month-old rats were surgically implanted with custom-built multisite microdrive arrays that allow targeting of multiple brain regions and independent adjustment of 18 individual tet-

rodes. The coordinates of the simultaneously targeted brain structures were as follows (bregma, lateral) in mm: (1) medial prefrontal cortex: two groups of tetrodes centered at (+4.2, +0.5), (+2.6, +0.5); (2) hippocampus: two groups of tetrodes centered at (-3.6, +2.2), (-6.0, +5.4) targeting the CA1 subfield. Individual tetrodes were lowered to their targets in very small increments over the course of several days and further adjusted in order to maximize unit yield, isolation, and stability. The signal from each channel of each tetrode was first buffered at a head-stage preamplifier, analog filtered, and differentially amplified (300 Hz–9 kHz for unit recordings, 0.1 Hz–475 Hz for LFP recordings). Signals were referenced against area-specific dedicated electrodes positioned to minimize local unit activity. The amplifier outputs were sampled at 31.25 kHz (unit) or 1.5 kHz (LFP) and stored to disk for offline analysis. Single-unit activity was isolated on the basis of spike waveform amplitude recorded on each of the four tetrode channels. Single units were counted for each behavioral epoch. A conservative estimate of unique single units was obtained by counting units recorded from the same tetrode over different behavioral epochs or days only once, i.e., on one given day and epoch. The LFP signal used to extract the theta rhythm was always derived from the same tetrode in each animal and was selected solely on the basis of the robustness of the theta component. The narrow distribution of hippocampal preferred phases shown in Figure 2G indicates a relative consistency in the phase relationships of the LFP signals used for the analysis.

LFP Filtering

Hippocampal LFP traces were band-pass filtered in the θ band (4–10 Hz) using digital filters constructed via the Parks-McClellan optimal equiripple FIR filter design. Transition bands were 4 Hz–4.5 Hz and 10 Hz–10.5 Hz. Maximal ripple was 0.05 in the stop bands and 0.01 in the pass band. In order to faithfully preserve the theta wave shape in the filtered trace, a wider band-pass filter was also employed in conjunction with the subset of decomposition methods utilizing zero crossings outlined below. In this case, the transition bands were 4 Hz–4.5 Hz and 40 Hz–40.5 Hz with 0.01 maximal ripple in the stop and pass bands.

Instantaneous Amplitude/Phase Decomposition

Seven alternative methods were used to decompose the filtered LFP $y(t)$ into instantaneous amplitude $\rho(t)$ and phase $\phi(t)$ components such that $y(t) = \text{Re}(\rho(t)e^{j\phi(t)})$. In all but one method, the instantaneous amplitude and phase were defined for a subset of special points in time, and the rest of the values were obtained by linear interpolation. In the *minima* method, the special points were the troughs of $y(t)$ identified as the negative to positive zero crossings of the derivative dy/dt , and they were assigned instantaneous phase of $-\pi$ radians. In the *maxima* method, the special points were the peaks identified as the positive to negative zero crossings of dy/dt and were assigned instantaneous phase of 0 radians. In the *extrema* method, both peaks and troughs were identified and assigned corresponding phase values as above. Analogously, in the *up* and *down* methods the special points were the negative to positive and positive to negative zero crossings of $y(t)$, and they were assigned instantaneous phases of $-\pi/2$ and $\pi/2$ radians, respectively. In the *zero crossing* method, both types of zero crossings were identified and assigned corresponding phase values. The instantaneous amplitude at extrema was set to $|y(t)|$, while at zero crossings it was set to a value that equated the power of $y(t)$ and the approximating signal over the half cycle centered at the zero crossing. Finally, in the *analytic signal* method the Hilbert transform $y_H(t)$ of $y(t)$ was computed, and the analytic signal $z(t) = y(t) + jy_H(t) = \rho(t)e^{j\phi(t)}$ provided instantaneous amplitude and phase values everywhere.

The methods above have different combinations of advantages and drawbacks. The major advantage of the analytic signal decomposition is that it is exact in the sense that $y(t) = \text{Re}(\rho(t)e^{j\phi(t)})$ for all t and has differentiable instantaneous phase and angular frequency. Yet the phase values at extrema and zeros are not guaranteed to be what one would expect (i.e., $-\pi$, 0, and $\pm\pi/2$), and the angular frequency can take on negative values. Furthermore, since the decomposition is exact even when the input contains a mixture

of signal and noise, both enter the instantaneous phase and amplitude components, and thus any denoising must occur at the earlier filtering step. This dictates the use of narrow band filters in conjunction with this method that can distort the input signal waveform. The remaining methods can be seen as fitting parametric models of reduced complexity to the input signal. The representations are exact only at their corresponding subsets of special points, and both phase and amplitude components are piecewise linear, thus sacrificing differentiability and continuity at special points of the instantaneous phase and angular frequency, respectively. The susceptibility of this class of methods to noise depends on the reliability with which special points can be identified, which in turn depends on the shape of the input signal. Therefore, they offer robust estimates of instantaneous phase and amplitude only in combination. Finally, the uniformity of the underlying phase value distribution ϕ_U is guaranteed only for methods that define one special point per wave cycle, i.e., *minima*, *maxima*, *up*, and *down*. The use of multiple methods for phase extraction makes subsequent analysis robust to signal deviation from model assumptions.

Effects of Theta Waveform Asymmetry

Depending on the method employed for obtaining the instantaneous phase, $\phi(t)$, subtle complications can arise in the presence of the theta waveform asymmetry. To see why this is the case, consider a fictitious sawtooth theta waveform with peak-to-trough time longer than trough-to-peak time, and a cell whose spikes are randomly distributed in time. Because of the asymmetry of the above waveform, more of the spikes will occur during the falling half of the theta cycle, leading to a nonuniform phase value distribution and an incorrect quantification of the phase locking properties of the cell.

The above problem is not merely of theoretical interest, as the experimentally observed theta waves indeed have an asymmetric sawtooth shape (Buzsaki et al., 1985; Buzsaki, 2002). The presence and form of the asymmetry depend on the precise position of the electrode, the behavior of the animal, and the method used to extract the instantaneous phase function $\phi(t)$ from the theta-filtered LFP trace. The consequences of the asymmetry for phase locking analysis can be explicitly evaluated by examining the underlying distribution of phase values, ϕ_U , obtained through uniform sampling of $\phi(t)$ (see below). Deviations from uniformity in ϕ_U as small as 2% can produce false positive phase locking detection in excess of 10% at $p = 0.01$ for an untuned unit with mean firing rate of 5 Hz recorded over a period of an hour. The false positive rate grows with the number of recorded spikes, which can be high not only because of a high mean firing rate, but also because of a long recording duration. Ultimately, for a sufficiently large number of spikes the error will approach 100%. Our analysis accounts for theta waveform asymmetry as described below.

Phase Value Distributions ϕ_U and ϕ_S

The amplitude-phase decomposition yields phase values $\phi(t)$ at the sample times $U = \{t = k\Delta t \mid k \in \{1, 2, \dots, T\}\}$, where $\Delta t \approx 0.67$ ms is the sampling period, and $T\Delta t$ is the duration of the recording. The underlying phase value distribution is defined as $\phi_U = \{\phi(t) \mid t \in U\}$. If a unit has generated N spikes at times $S = \{\tau_k \mid k \in \{1, 2, \dots, N\}\}$, its phase value distribution is given by $\phi_S = \{\phi(t) \mid t \in S\}$. Thus, ϕ_S can be regarded as a sample drawn from ϕ_U .

Comparing ϕ_U and ϕ_S

If S is a random sample of U , then ϕ_S will replicate ϕ_U . In particular, if ϕ_U is uniform, then under random sampling so is ϕ_S . Uniformity of ϕ_U is particularly desirable, because in this case the question of phase locking detection reduces to simply detecting departures from uniformity in ϕ_S , which is readily done by the tools of circular statistics.

Fortunately, we can devise a transformation $\Psi : [-\pi, \pi] \rightarrow [-\pi, \pi]$ such that $\phi_U^{\Psi} = \Psi(\phi_U) = \{\Psi(x) \mid x \in U\}$ is uniform. If we similarly let $\phi_S^{\Psi} = \Psi(\phi_S) = \{\Psi(x) \mid x \in S\}$ be the Ψ -transformed unit phase value distribution, then testing for the presence of phase locking amounts to testing whether ϕ_S^{Ψ} is uniform. To ease notation, we use ϕ_S to refer to the Ψ -transformed unit phase value distribution.

Let $F_U : [-\pi, \pi] \rightarrow [0, 1]$ be the empirical cumulative distribution

function corresponding to ϕ_U . Then, $\Psi(x) = 2\pi F_U(x) - \pi$ yields the desired transformation. This transformation is equivalent to the computation of the *circular ranks* or *uniform scores* of the elements of ϕ_U . Clearly, if ϕ_U is uniform to begin with, Ψ reduces to the identity map.

Phase Locking Detection and Characterization

The presence of phase locking was evaluated by applying the Rayleigh test for circular uniformity on the Ψ -transformed unit phase value distribution ϕ_S . Briefly, given n phase values ϕ_i define the first trigonometric moment $m' = (1/n) \sum_{i=1}^n e^{j\phi_i} = \bar{R}e^{j\mu}$. The sample mean direction or preferred phase μ is given by the orientation of m' , while the mean resultant length \bar{R} is given by the modulus of m' . The Rayleigh statistic is $Z = n\bar{R}^2$, and the probability that the null hypothesis of sample uniformity holds is given by $P = e^{-Z} [1 + (2Z - Z^2)/(4n) - (24Z - 132Z^2 + 76Z^3 - 9Z^4)/(288n^2)]$. For $n > 50$, the approximation $P = e^{-Z}$ is adequate (Fisher, 1993; Zar, 1998; Mardia, 1972). All significantly phase-locked units were fit with a von Mises distribution with density $f(\phi) = [1/(2\pi I_0(\kappa))] e^{\kappa \cos(\phi - \mu)}$, for $-\pi \leq \phi < \pi$ and $0 \leq \kappa < \infty$. The maximum likelihood (ML) estimate for the von Mises mean direction parameter is equal to the sample mean direction μ . The ML estimate for the concentration parameter κ is given by the solution of the equation $I_1(\kappa)/I_0(\kappa) = \bar{R}$, where $I_i(x)$ is the modified Bessel function of order i . The solution was obtained by using a numerical zero finding routine.

Cross-Covariance Analysis

In order to quantify the interactions between pairs of simultaneously recorded spike trains, we considered each pair to be the realization of a stationary bivariate stochastic point process (N_i, N_j) , where $N_i(t)$ indicates the number of spikes generated by neuron i in the time interval from 0 to t (Perkel et al., 1967a; Perkel et al., 1967b). The differential increment at time t is defined as $dN(t) = (N(t + dt) - N(t))$ and counts the number of events in the small interval $(t, t + dt]$. For an orderly point process, $dN(t)$ takes the values of zero or one, depending on whether or not a spike has occurred in the time interval between t and $t + dt$. The mean intensity P_i of the point process N_i is defined as $E\{dN_i(t)\} = P_i dt$, and corresponds to the mean firing rate in the units of the time axis. The cross-product density at lag u , $P_{ij}(u)$, between the point processes N_i and N_j is defined as $E\{dN_i(t + u)dN_j(t)\} = P_{ij}(u)du$ and can be interpreted as the probability of co-occurrence of a N_j event in the interval $(t + u, t + u + du]$ and a N_i event in $(t, t + dt]$ (Brillinger, 1976; Halliday and Rosenberg, 1999). Finally the cross-covariance function, $q_{ij}(u)$, defined as $\text{cov}\{dN_i(t + u)dN_j(t)\} = q_{ij}(u)du$ can be expressed as $q_{ij}(u) = P_{ij}(u) - P_i P_j$. If the two spike trains are independent, $P_{ij}(u) = P_i P_j$ and consequently $q_{ij}(u) = 0$. Therefore, the null hypothesis, H_0 , of no interaction between N_i and N_j can be rejected if an estimate $\hat{q}_{ij}(u)$ of the cross-covariance function deviates significantly from 0.

We estimated the cross-covariance function between spike trains N_i and N_j in the time domain on the basis of the *cross-correlation histogram*, $J_{ij}^{a,b}(u)$, which counts the number of spike pairs occurring at times (τ_{im}, τ_{jn}) , such that $|\tau_{im} - \tau_{jn} - u| < b/2$, with b specifying the bin size and T specifying the period of observation. We used the cross-covariance estimate $\hat{q}_{ij}(u) = J_{ij}^{a,b}(u)/(bT) - \hat{P}_i \hat{P}_j$, where $\hat{P}_i = N_i(T)/T$ and $\hat{P}_j = N_j(T)/T$ (Brillinger, 1976; Halliday and Rosenberg, 1999). The asymptotic distribution of $\hat{q}_{ij}(u)$ is approximately normal $N_{\{\mu, \sigma^2\}} = q_{ij}(u), \sigma^2 = P_{ij}(u)/(bT)$ (Halliday and Rosenberg, 1999) and consequently under the null hypothesis H_0 of spike train independence $\hat{q}_{ij}(u) \sim N\{\mu = 0, \sigma^2 = P_i P_j / bT\}$. Since the variance of $\hat{q}_{ij}(u)$ under H_0 depends on the mean firing rates, bin size, and period of observation, we used a standardized cross-covariance, $Q_{ij}(u) = \sqrt{bT/P_i P_j} \hat{q}_{ij}(u)$, so that $Q_{ij}(u) \sim N\{\mu = 0, \sigma^2 = 1\}$ under H_0 . Therefore, H_0 could be rejected when $|Q_{ij}(u)| > Z_{\alpha(2)}$ for some u , where $Z_{\alpha(2)} = \sqrt{2} \text{erf}^{-1}(1 - \alpha)$ is the two-tailed critical z value at level α . Standardizing the cross-covariance estimates allowed us to meaningfully compare, combine, and display $Q_{ij}(u)$ on a common scale.

We computed $Q_{ij}(u)$ for all 3617 pairs of simultaneously recorded prefrontal and hippocampal units, over time lags u between -512 and $+512$ ms in 1 ms steps using a 15 ms bin. Thus, for each pair of spike trains, $Q_{ij}(u)$ was a sequence of 1025 values. Since H_0 could be rejected at each lag, we lowered our target $\alpha = 0.01$ by

1025, giving a lag-corrected critical z value of 4.42. Under these conditions, 948 or 26% of the pairs were deemed to have significant interactions. However, this treatment is only asymptotically correct and for spike trains with small numbers of events can produce spurious significant correlations. To see why this is the case, note that under the null hypothesis $J_{ij}^{T,b}(u) \sim \text{Poisson}(\lambda = bTP_iP_j)$ (Brillinger, 1976), and $Q_{ij}(u)$ can be expressed as $Q_{ij}(u) = (J_{ij}^{T,b}(u) - \hat{\lambda})/\sqrt{\hat{\lambda}}$, where $\hat{\lambda} = bT\hat{P}_i\hat{P}_j$. Thus, $Q_{ij}(u)$ can be viewed as a standardized cross-correlation histogram, and $Q_{ij}(u)$ is approximately normal when the normal approximation to the Poisson distribution applies, i.e. for $\lambda > 20$, which gives the condition $bT\hat{P}_i\hat{P}_j > 20$. Given a recording duration T of 30 min and bin size b of 15 ms, the product of the firing rates in Hz must exceed 0.74 in order for the approximation to apply. Since about half of the recorded units had mean firing rates under 0.74 Hz, spurious significant cross-covariance functions were seen, displaying characteristic narrow peaks and troughs (width in the order of b , i.e., 15 ms). Spurious $Q_{ij}(u)$ could be eliminated by restricting the cross-covariance analysis only to the 708 spike train pairs with sufficiently high mean firing rates. Under these conditions, 134 or 19% of the qualifying pairs had significant interactions. However, this restriction disqualified almost 51% of the prefrontal units from entering the analysis. Therefore, instead of biasing the analysis by imposing minimal firing rate restrictions, we accepted possibly spurious $Q_{ij}(u)$, with the understanding that they could only contribute unstructured noise that would be attenuated in subsequent averaging. This was explicitly verified by repeating the analysis with the minimal firing rate restriction imposed.

The standardized mean cross-covariance, $Q_i(u)$, between prefrontal unit i and the simultaneously recorded population of hippocampal units was computed as $Q_i(u) = (1/\sqrt{K})\sum_{j=1}^K Q_{ij}(u)$ where the index j ran over the K hippocampal units exhibiting significant interactions with i . The $1/\sqrt{K}$ factor was applied so that $Q_i(u)$ was approximately normal $N(\mu = 0, \sigma^2 = 1)$ under the null hypothesis of independence between N_i and all N_j . The mean squared cross-covariance, $Q_i^2(u)$, was computed $Q_i^2(u) = (1/K)\sum_{j=1}^K Q_{ij}^2(u)$. This measure controlled for the possible cancellation of significant but opposite covariance structure allowed by $Q_i(u)$. When $Q_i(u)$ or $Q_i^2(u)$ were averaged over a subset L of prefrontal units, the resulting quantities were denoted as $\langle Q_i(u) \rangle_L = (1/L)\sum_i Q_i(u)$, with an analogous expression for $\langle Q_i^2(u) \rangle_L$.

We also repeated the entire analysis based on cross-covariance estimates constructed in the frequency domain as the inverse Fourier transform of the cross-spectrum, computed using the method of disjoint sections (Halliday et al., 1995). All results that we report here were qualitatively unaffected by the estimation procedure.

Acknowledgments

We thank John Dani, Peter Dayan, Gilles Laurent, Albert Lee, Kenway Louie, Stelios Smirnakis, Andreas Tolias, and Casimir Wierzynski for many useful discussions and comments on the manuscript. This work was supported by a 21st Century McDonnell Foundation Award, an Alfred P. Sloan Research Fellowship, the Bren Foundation, the Gimbel Discovery Fund (A.G.S.), and a Pauline Whiteman Fellowship (E.V.L.).

Received: November 18, 2004

Revised: January 14, 2005

Accepted: February 27, 2005

Published: April 6, 2005

References

Alonso, A., and Garcia-Austt, E. (1987). Neuronal sources of theta rhythm in the entorhinal cortex of the rat. II. Phase relations between unit discharges and theta field potentials. *Exp. Brain Res.* **67**, 502–509.

Bassant, M., and Poindessous-Jazat, F. (2001). Ventral tegmental nucleus of Gudden: a pontine hippocampal theta generator? *Hippocampus* **11**, 809–813.

Bontempi, B., Laurent-Demir, C., Destrade, C., and Jaffard, R. (1999). Time-dependent reorganization of brain circuitry underlying long-term memory storage. *Nature* **400**, 671–675.

Brillinger, D. (1976). Measuring the association of point processes: a case history. *Am. Math. Mon.* **83**, 16–22.

Buzsaki, G. (2002). Theta oscillations in the hippocampus. *Neuron* **33**, 325–340.

Buzsaki, G., and Eidelberg, E. (1983). Phase relations of hippocampal projection cells and interneurons to theta activity in the anesthetized rat. *Brain Res.* **266**, 334–339.

Buzsaki, G., Rappelsberger, P., and Kellenyi, L. (1985). Depth profiles of hippocampal rhythmic slow activity ('theta rhythm') depend on behaviour. *Electroencephalogr. Clin. Neurophysiol.* **61**, 77–88.

Chapman, C., and Lacaille, J. (1999). Intrinsic theta-frequency membrane potential oscillations in hippocampal CA1 interneurons of stratum lacunosum-moleculare. *J. Neurophysiol.* **81**, 1296–1307.

Colom, L., Christie, B., and Bland, B. (1988). Cingulate cell discharge patterns related to hippocampal EEG and their modulation by muscarinic and nicotinic agents. *Brain Res.* **460**, 329–338.

Degenetais, E., Thierry, A., Glowinski, J., and Gioanni, Y. (2003). Synaptic influence of hippocampus on pyramidal cells of the rat prefrontal cortex: an in vivo intracellular recording study. *Cereb. Cortex* **13**, 782–792.

Ferino, F., Thierry, A., and Glowinski, J. (1987). Anatomical and electrophysiological evidence for a direct projection from Ammon's horn to medial prefrontal cortex. *Exp. Brain Res.* **65**, 421–426.

Fisher, N. (1993). *Statistical Analysis of Circular Data* (Cambridge: Cambridge University Press).

Fletcher, P., and Henson, R. (2001). Frontal lobes and human memory: insights from functional neuroimaging. *Brain* **124**, 849–881.

Floresco, S., Seamans, J., and Phillips, A. (1997). Selective roles for hippocampal, prefrontal cortical, and ventral striatal circuits in radial-arm maze tasks with or without a delay. *J. Neurosci.* **17**, 1880–1890.

Fox, S., Wolfson, S., and Ranck, J. (1986). Hippocampal theta rhythm and the firing of neurons in walking and urethane anesthetized rats. *Exp. Brain Res.* **62**, 495–508.

Frankland, P., Bontempi, B., Talton, L., Kaczmarek, L., and Silva, A. (2004). The involvement of the anterior cingulate cortex in remote contextual fear memory. *Science* **304**, 881–883.

Fuster, J. (1997). *The Prefrontal Cortex: Anatomy, Physiology, and Neuropsychology of the Frontal Lobe*, Third Edition (Philadelphia: Lippincott-Raven).

Gambini, J., Velluti, R., and Pedemonte, M. (2002). Hippocampal theta rhythm synchronizes visual neurons in sleep and waking. *Brain Res.* **926**, 137–141.

Green, J., and Arduini, A. (1954). Hippocampal electrical activity in arousal. *J. Neurophysiol.* **17**, 533–557.

Halliday, D., and Rosenberg, J. (1999). Time and frequency domain analysis of spike train and time series data. In *Modern Techniques in Neuroscience Research*, U. Windhorst and H. Johansson, eds. (Berlin: Springer-Verlag), pp. 503–543.

Halliday, D., Rosenberg, J., Amjad, A., Breeze, P., Conway, B., and Farmer, S. (1995). A framework for the analysis of mixed time series/point process data—theory and application to the study of physiological tremor, single motor unit discharges and electromyograms. *Prog. Biophys. Mol. Biol.* **64**, 237–278.

Hu, H., Vervaeke, K., and Strom, J. (2002). Two forms of electrical resonance at theta frequencies generated by M-current, h-current and persistent Na⁺ current in rat hippocampal pyramidal cells. *J. Physiol.* **543**, 783–805.

Hutcheon, B., and Yarom, Y. (2000). Resonance, oscillation and the intrinsic frequency preferences of neurons. *Trends Neurosci.* **23**, 216–222.

Jay, T., Thierry, A., Wiklund, L., and Glowinski, J. (1992). Excitatory amino acid pathway from the hippocampus to the prefrontal cortex. Contribution of AMPA receptors in hippocampo-prefrontal cortex transmission. *Eur. J. Neurosci.* **4**, 1285–1295.

- Jay, T., Burette, F., and Laroche, S. (1995). NMDA receptor-dependent long-term potentiation in the hippocampal afferent fibre system to the prefrontal cortex in the rat. *Eur. J. Neurosci.* 7, 247–250.
- Kahana, M., Sekuler, R., Caplan, J., Kirschen, M., and Madsen, J. (1999). Human theta oscillations exhibit task dependence during virtual maze navigation. *Nature* 399, 781–784.
- Kocsis, B., and Vertes, R. (1992). Dorsal raphe neurons: synchronous discharge with the theta rhythm of the hippocampus in the freely behaving rat. *J. Neurophysiol.* 68, 1463–1467.
- Laroche, S., Jay, T., and Thierry, A. (1990). Long-term potentiation in the prefrontal cortex following stimulation of the hippocampal CA1 subicular region. *Neurosci. Lett.* 114, 184–190.
- Laroche, S., Davis, S., and Jay, T. (2000). Plasticity at hippocampal to prefrontal cortex synapses: dual roles in working memory and consolidation. *Hippocampus* 10, 438–446.
- Leung, L., and Yu, H.-W. (1998). Theta-frequency resonance in hippocampal CA1 neurons in vitro demonstrated by sinusoidal current injection. *J. Neurophysiol.* 79, 1592–1596.
- Mardia, K. (1972). *Statistics of Directional Data* (New York: Academic Press).
- Markram, H., Lubke, J., Frotscher, M., and Sakmann, B. (1997). Regulation of synaptic efficacy by coincidence of postsynaptic APs and EPSPs. *Science* 275, 213–215.
- Maviel, T., Durkin, T., Menzaghi, F., and Bontempi, B. (2004). Sites of neocortical reorganization critical for remote spatial memory. *Science* 305, 96–99.
- Miller, R. (1991). *Cortico-Hippocampal Interplay and the Representation of Contexts in the Brain* (Berlin: Springer-Verlag).
- Natsume, K., Hallworth, N., Szgatti, T., and Bland, B. (1999). Hippocampal theta-related cellular activity in the superior colliculus of the urethane-anesthetized rat. *Hippocampus* 9, 500–509.
- Pare, D., and Gaudreau, H. (1996). Projection cells and interneurons of the lateral and basolateral amygdala: distinct firing patterns and differential relation to theta and delta rhythms in conscious cats. *J. Neurosci.* 16, 3334–3350.
- Pedemonte, M., Pena, J., and Velluti, A. (1996). Firing of inferior colliculus auditory neurons is phase-locked to the hippocampus theta rhythm during paradoxical sleep and waking. *Exp. Brain Res.* 112, 41–46.
- Pedemonte, M., Perez-Perera, L., Pena, J., and Velluti, R. (2001). Sleep and wakefulness auditory processing: cortical units vs. hippocampal theta rhythm. *Sleep Res. Online* 4, 51–57.
- Perkel, D., Gerstein, G., and Moore, G. (1967a). Neuronal spike trains and stochastic point processes. I. The single spike train. *Biophys. J.* 7, 391–418.
- Perkel, D., Gerstein, G., and Moore, G. (1967b). Neuronal spike trains and stochastic point processes. II. Simultaneous spike trains. *Biophys. J.* 7, 419–440.
- Roberts, P., and Bell, C. (2002). Spike timing dependent synaptic plasticity in biological systems. *Biol. Cybern.* 87, 392–403.
- Squire, L. (1992). Memory and the hippocampus: A synthesis from findings with rats, monkeys, and humans. *Psychol. Rev.* 99, 195–231.
- Swanson, L. (1981). A direct projection from Ammon's horn to prefrontal cortex in the rat. *Brain Res.* 217, 150–154.
- Takehara, K., Kawahara, S., and Kirino, Y. (2003). Time-dependent reorganization of the brain components underlying memory retention in trace eyeblink conditioning. *J. Neurosci.* 23, 9897–9905.
- Takita, M., Izaki, Y., Jay, T., Kaneko, H., and Suzuki, S. (1999). Induction of stable long-term depression in vivo in the hippocampal prefrontal pathway. *Eur. J. Neurosci.* 11, 4145–4148.
- Thierry, A., Gioanni, Y., Degenetais, E., and Glowinski, J. (2000). Hippocampo-prefrontal cortex pathway: anatomical and electrophysiological characteristics. *Hippocampus* 10, 411–419.
- Tierney, P., Degenetais, E., Thierry, A., Glowinski, J., and Gioanni, Y. (2004). Influence of the hippocampus on interneurons of the rat prefrontal cortex. *Eur. J. Neurosci.* 20, 514–524.
- Vanderwolf, C. (1969). Hippocampal electrical activity and voluntary movement in the rat. *Electroencephalogr. Clin. Neurophysiol.* 26, 407–418.
- Vinogradova, O., and Brazhnik, E. (1977). Theta-bursts of hippocampal and septal neurons. *Zh. Vyssh. Nerv. Deiat. Im. I P Pavlova* 27, 1166–1172.
- Wilson, M., and McNaughton, B. (1993). Dynamics of the hippocampal ensemble code for space. *Science* 261, 1055–1058.
- Wiltgen, B., Brown, R., Talton, L., and Silva, A. (2004). New circuits for old memories: the role of the neocortex in consolidation. *Neuron* 44, 101–108.
- Zar, J. (1998). *Biostatistical Analysis, Fourth Edition* (Upper Saddle River, NJ: Prentice Hall).